ACSNANO
www.acsnano.org
ARTICLE

Biaxial Dielectrophoresis Force Spectroscopy: A Stoichiometric Approach for Examining Intermolecular Weak Binding Interactions

In Soo Park,[†,▼] Tae Joon Kwak,[‡,▼] Gyudo Lee,[§] Myeonggu Son,[†] Jeong Woo Choi,[†] Seungyeop Choi,[†] Kihwan Nam,[∥] Sei-Young Lee,[†] Woo-Jin Chang,[‡] Kilho Eom,[⊥] Dae Sung Yoon,[#] Sangyoup Lee,[∥,¶] Rashid Bashir,[△] and Sang Woo Lee*[,†]

[†]Department of Biomedical Engineering, Yonsei University, Wonju 220-710, Korea
[‡]Mechanical Engineering Department, University of Wisconsin—Milwaukee, Milwaukee, Wisconsin 53211, United States
[§]T.H. Chan School of Public Health, Harvard University, Boston, Massachusetts 02115, United States
[∥]Biomedical Research Institute, Korea Institute of Science and Technology, Seoul 136-791, Korea
[⊥]Biomechanics Laboratory, College of Sport Science, Sungkyunkwan University, Suwon 440-746, Korea
[#]Department of Bio-convergence Engineering, Korea University, Seoul 136-703, Korea
[¶]Department of Biomedical Engineering, University of Science and Technology, Daejeon 305-350, Korea
[△]Department of Bioengineering, Micro and Nanotechnology Laboratory, University of Illinois at Urbana—Champaign Champaign, Illinois 61801, United States

S *Supporting Information*

ABSTRACT: **The direct quantification of weak intermolecular binding interactions is very important for many applications in biology and medicine. Techniques that can be used to investigate such interactions under a controlled environment, while varying different parameters such as loading rate, pulling direction, rupture event measurements, and the use of different functionalized probes, are still lacking. Herein, we demonstrate a biaxial dielectrophoresis force spectroscopy (BDFS) method that can be used to investigate weak unbinding events in a high-throughput manner under controlled environments and by varying the pulling direction (*i.e.*, transverse and/or vertical axes) as well as the loading rate. With the BDFS system, we can quantitatively analyze binding interactions related to hydrogen bonding or ionic attractions between functionalized microbeads and a surface within a microfluidic device. Our BDFS system allowed for the characterization of the number of bonds involved in an interaction, bond affinity, kinetic rates, and energy barrier heights and widths from different regimes of the energy landscape.**

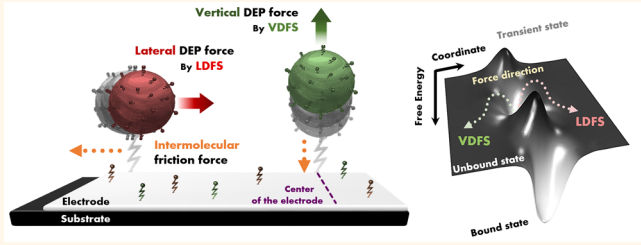

KEYWORDS: *dielectrophoresis force spectroscopy, intermolecular weak binding interactions, energy landscape, microfluidic device, pulling direction*

Noncovalent weak molecular interactions including hydrogen bonds, van der Waals forces, electrostatic attraction/repulsion, and hydrophobic interactions play an essential role in a wide range of biological processes ranging from molecular recognition to cell motility.[1] Quantifying these weak binding forces involved in molecular interactions can yield fundamental information that can explain how molecular interactions occur and their interplay with each other in biochemical processes. For a decade, force spectroscopy (FS), for example, fluorescent resonance energy transfer,[2] atomic force microscopy,[3,4] optical tweezers,[5,6] and magnetic tweezers,[7] has enabled quantitative understanding of molecular interactions including DNA/RNA interactions, methylation,[8] ligand−receptor binding affinity on cell surfaces,[9,10] and protein folding/unfolding.[11−13] In general, FS methods need more than several hundred measurements for statistical analysis of the ensemble average of physical quantities such as forces and end-to-end distances.[13] For instance, the ensemble average of forces required for protein unfolding has to be measured under different pulling regimes ranging from the quasi-equilibrium to

Received: August 24, 2015
Accepted: March 3, 2016

DOI: 10.1021/acsnano.5b05286
ACS Nano XXXX, XXX, XXX−XXX

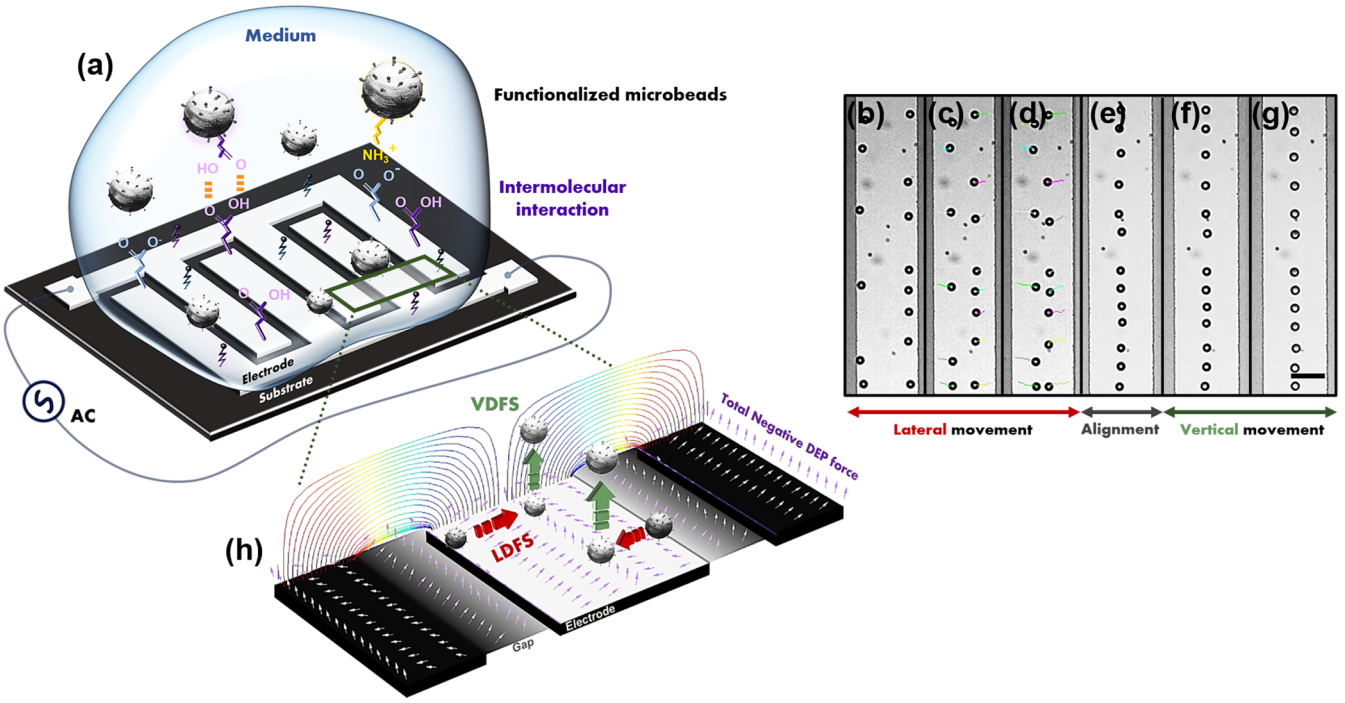

Figure 1. Concept of the BDFS system. (a) Schematic illustration of BDFS. (b–g) Time-lapse optical images exhibit how BDFS works as a combination of LDFS and VDFS. Ten micrometer polystyrene microbeads are aligned on the edge of the electrode by positive DEP force acting on the beads by applying 50 $V_{p\text{-}p}$ at 1 kHz and are moved toward the center of the electrode by LDFS and stopped at a certain position on the electrode with the application of 27 $V_{p\text{-}p}$ AC with 1 MHz (negative DEP force acting on the beads) (b–d), used for LDFS. When the magnitude of the applied AC increases to 35 $V_{p\text{-}p}$, the microbeads are aligned at the center of electrode (e). As the magnitude is increased, the microbeads are levitated (f,g), used for VDFS. The scale bar is 40 μm, and the time interval is 20 s. (h) Simulation results depict electric field intensity at the IDT electrode in a microfluidic chip. For negative DEP forces on the overall IDT electrode, microbeads are aligned at the center of electrode by lateral DEP forces and are trapped and levitated simultaneously by the vertical DEP force.

non-equilibrium state. As such, an ensemble average provides information with regard to the free energy landscape of weak binding interactions.[14,15] Furthermore, rupture forces and energy landscapes can vary due to slight changes in experimental conditions such as pulling directions,[16−18] loading rates,[19,20] temperatures,[21] and stiffness constant (defined as $\Delta F/\Delta x$) of the force probe.[16−22] Considerable progress has also been made in investigating the rupture force and energy landscape pathway mechanism for each condition.[16−22] However, there is no method to examine the rupture force and energy landscape of weak binding interactions by perturbing the free energy landscape with more than one variable (*e.g.*, loading rate and pulling direction at the same time) under the same environment, as these variables can have individual as well as combined effects which are very important toward understanding biological processes in living systems.

Recently, we have developed a new force spectroscopy measurement approach called dielectrophoretic (DEP) tweezers, where hundreds of polymeric microbeads are used as probes to measure intermolecular binding forces.[23−25] This is a promising technique due to the low cost of microfluidic chips, simple operating procedures, and the high precision measurement of intermolecular forces. Since this measurement technique can apply loading rates that can vary from the quasi-equilibrium state (extremely low loading rate) to the non-equilibrium state (high loading rate), energy landscapes of a certain ligand−receptor interaction can be investigated by measuring high-throughput unbinding events simultaneously with a wide range of loading rates.[25] However, the DEP tweezers approach reported before allows only an examination of intermolecular forces in the vertical direction (and hence could be termed "vertical DEP force spectroscopy", VDFS) and did not examine the force interactions when the loading and pulling is in the horizontal or transverse direction.

As force interaction measurements are important to measure in both vertical and horizontal directions (parallel and transverse directions to the molecular orientations), here we report the development of a biaxial DEP force spectroscopy (BDFS) method, which can be used to investigate the rupture force of noncovalent interactions between single functional groups through "lateral" and "vertical" movement of microbeads used as probes in microfluidic devices. We show that lateral DEP force spectroscopy (termed LDFS) can examine intermolecular forces as the microbeads are moved along the electrode, where the magnitude of DEP force is gradually decreased from the edge to the center of the electrode. This means that a loading rate gradient is formed naturally in the lateral direction. Using our new biaxial DEP force spectroscopy measurement, both vertical (VDFS) and lateral (LDFS) loading can also be applied sequentially under the same exact conditions. We first demonstrated the high-throughput measurement of hydrogen bond and ionic interaction between single functionalized group as a model inside a microfluidic device, by sequentially applying the two different pulling directions as well as different loading rates. From this demonstration, we observed that bond numbers involved in the rupture event, bond affinity, and dissociation rate of the weak intermolecular interactions depend on pulling directions as well as loading rates. Our approach can be used to gain a better understanding of the effect of the pulling direction and

DOI: 10.1021/acsnano.5b05286
ACS Nano XXXX, XXX, XXX−XXX

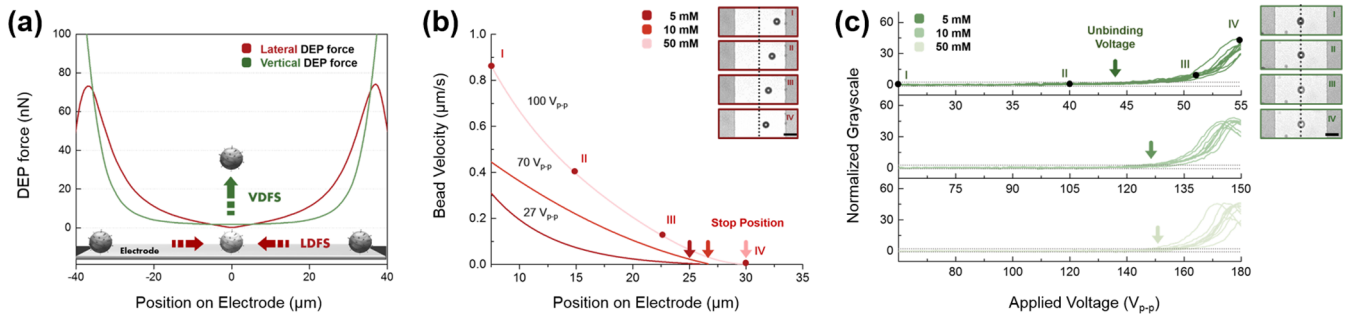

Figure 2. Finite element analysis of BDFS, lateral movement displacement, and grayscale height variation graph. (a) Parallel plot of simulated vertical and lateral dielectrophoresis forces at 5 μm heights from the edge of the electrode to the center as 100 V_{p-p} was applied. (b,c) Hydrogen interaction between carboxyl-terminated beads and the carboxyl-functionalized oxide surface at pH 4 with 5, 10, and 50 mM concentrations. Scale bar (inset) is 20 μm. (b) Lateral movement velocity graph as a function of electrode position for LDFS as the applied voltages were 27, 70, and 100 V_{p-p}. (c) Grayscale height variation graph as a function of applied voltage for VDFS.

loading rate on intermolecular interactions with regard to mechanical and chemical kinetics.

RESULTS

Observation of Bead Behavior in the BDFS System. First, the movement of 10 μm polystyrene microbeads coated with carboxyl or amino functional groups on carboxyl-functionalized silicon dioxide surfaces was observed by applying DEP forces. These forces were generated *via* the introduction of AC signals to interdigitated (IDT) electrodes located beneath the silicon dioxide layer. Before the AC signal was applied, interaction between the beads and the functionalized oxide surface occurred with hydrogen bonds (carboxyl-terminated beads and carboxyl-terminated surfaces at pH 4) or electrical attractions (amino-terminated beads and carboxyl-terminated surfaces at pH 7). van der Waals interactions between the beads and the functionalized surface were neglected, indicating that the bond force is much smaller than the hydrogen and ionic bond force. Additionally, hydrophobic interactions could be also ignored because, even though the polystyrene beads may be hydrophobic, the oxide surface is hydrophilic (Supporting Figure S1).[24,25] Figure 1a presents a schematic diagram of the measurement system, in which an AC signal was applied to the electrode (see also Supporting Movie M1). The beads were aligned on the edge of the electrode, which is the position that starts a lateral movement, by positive DEP force acting on the beads (Figure 1b). Since the beads should not be moved vertically from the functionalized surface but be moved laterally through the surface by the negative DEP force, we carefully controlled the magnitude of the applied voltage. As a result, the beads on the functionalized silicon dioxide substrate were moved laterally toward the center of the electrode and stopped at a certain position on the surface (Figure 1b–d). The beads were sequentially aligned at the center of the electrodes (Figure 1e) and were moved upward from the silicon dioxide surface (Figure 1f,g). These observations were also verified *via* the grayscale measurement method that we reported in a prior study (see also Supporting Figure S2).[25] In order to investigate the lateral movement of the bead, the motion of each bead was closely observed, and we found that the beads rolled across the functionalized silicon dioxide surface when lateral movements were initiated *via* the lateral DEP force (Supporting Figure S3).

Finite Element Analysis Based Simulation. To quantitatively characterize the lateral and vertical movement of the beads, a finite element analysis (FEA) based simulation was performed (a detailed description of the simulation method can be found in Materials and Methods and Supporting Note N1 and Figure S5). Figure 2a represents the DEP force acting on a bead as a function of its position on the electrode. The DEP force was greater in the lateral direction than in the vertical direction (between 5 and 35 μm), as shown in Figure 2a. The bead was mainly controlled by lateral DEP forces until it reached the center of the electrode (Figure 1b–e) (Supporting Figure S2). Moreover, the DEP force in the vertical direction was insufficient to move the bead upward even after breaking the intermolecular interactions between the bead and the surface during the rolling of the beads across the electrodes.

Measurement of Physical Quantities Corresponding to Weak Binding Interaction Forces in BDFS. We explored the characteristics of hydrogen bonds and ionic binding interactions with the BDFS method as the concentration of carboxyl functional groups on the silicon dioxide surface was varied in conjunction with the magnitude of the applied voltage on the electrode located beneath the substrate surface. First, carboxyl-functionalized polystyrene beads (10 μm) were aligned with the edges of the electrodes, which were covered by the carboxyl-functionalized oxide surface in a microfluidic chip. The beads and oxide surface interacted *via* hydrogen bonding. Subsequently, when voltages were applied at 1 MHz, the beads that were at the edges began to move toward the center of the electrode and stopped at a certain position between the edge and the center of the electrode (*e.g.*, Figure 1b–d). These voltages were 27, 70, and 100 V_{p-p}, corresponding to the concentrations of 5, 10, and 50 mM of carboxyl groups used to functionalize the substrate surfaces, respectively. Furthermore, the velocity and the stopping position of the beads was calculated from imaging of their movement, as shown in Figure 2b. The microbeads stopped at different locations of the electrode depending on the density of the functional group. The stopping positions were 25.8 ± 0.64, 26.4 ± 1.29, and 30.71 ± 0.51 μm, corresponding to the three carboxyl concentrations, respectively (see Supporting Note N2 for the detailed method used to measure the stop positions). Voltages applied to align the beads at the center of the electrodes (*e.g.*, Figure 1e) were further increased to 35, 105, and 126 V_{p-p}, respectively. Sequentially, the hydrogen bond rupture conditions as measured *via* vertical DEP forces (*e.g.*, Figure 1f,g) were 42, 123, and 134 V_{p-p}, respectively, according to grayscale measurement data, as shown in Figure 2c.

DOI: 10.1021/acsnano.5b05286
ACS Nano XXXX, XXX, XXX–XXX

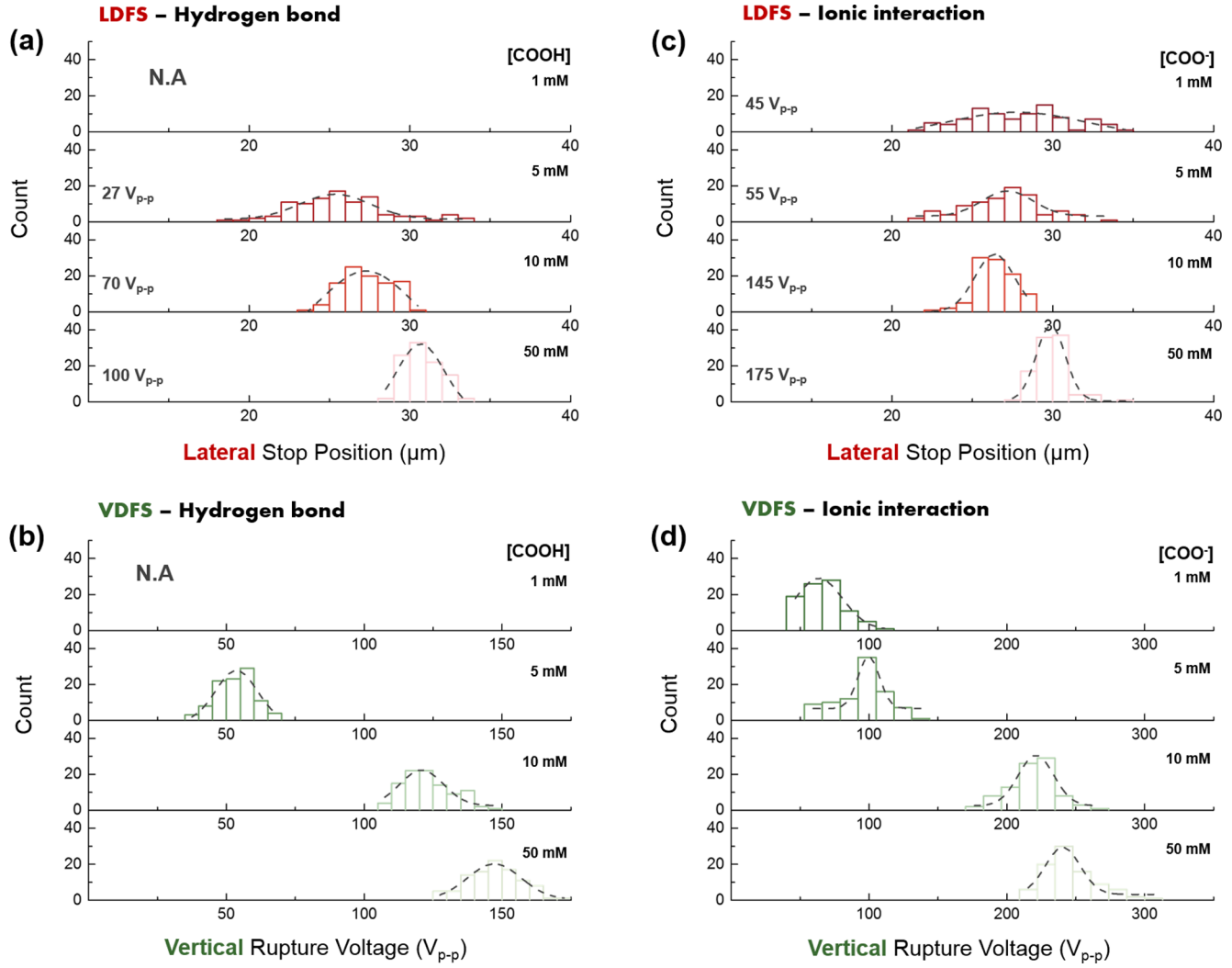

Figure 3. Histogram graph representing the number of the functionalized beads as a function of stop position and rupture voltage. (a,b) Hydrogen interaction between carboxyl-terminated beads and the carboxyl-functionalized oxide surface at pH 4 with 5, 10, and 50 mM concentrations: (a) stop position for LDFS; (b) rupture voltage for VDFS. (c,d) Electrostatic attraction (ionic) bond between amino-terminated beads and the carboxyl-functionalized oxide surface at pH 7 with 1, 5, 10, and 50 mM concentrations: (c) stop position for LDFS; (d) rupture voltage for VDFS.

Additionally, the ionic binding interactions were also examined *via* amino-functionalized beads and carboxyl-functionalized silicon dioxide surfaces using the same procedures described above. The voltages required to make the beads move from the edge to the center before stopping at a certain position were 55, 145, and 175 $V_{p\text{-}p}$ at the surface functional group concentrations of 5, 10, and 50 mM, respectively. As seen in Figure 2c, after the beads were aligned to the center of the electrode, the voltages necessary to rupture ionic binding interactions were measured to be 89, 218, and 246 $V_{p\text{-}p}$. The microbeads were also observed to stop at different locations of the electrode at 23.6 ± 0.88, 26.8 ± 0.82, and 29 ± 0.67 μm, respectively (Supporting Figure S6).

Multifunctional Probe Array in BDFS. Herein, we observed the lateral movement of more than hundreds of carboxyl-coated beads or amino-coated beads at the same time by applying lateral DEP forces in a microfluidic device. Sequentially, the vertical movements of these beads were also observed under the same environment in the microfluidic device as the applied voltage was varied. Furthermore, to remove the force loading effect in each measurement system when rupture occurred, the loading rate of the LDFS system closely matched that of the VDFS system as much as possible (see Supporting Note N3 for a detailed description of loading rates). Figure 3a reveals the distribution of stop positions measured by LDFS at different concentrations of surface functionalization when hydrogen-bond-mediated interactions occurred between carboxyl-coated beads and the carboxyl-functionalized surface. The voltages were measured to determine the rupture force of the hydrogen-bond-mediated interaction by VDFS, as shown in Figure 3b of the sequence. Moreover, Figure 3c,d also describes the stop positions and voltages at which rupture occurred as measured by BDFS, corresponding with the ionic binding interactions between amino-coated beads and the carboxyl-functionalized silicon dioxide surface.

DISCUSSION

In order to study the binding interactions between the beads and functionalized surfaces, we developed a sequential lateral and vertical movement method within the LDFS/VDFS measurement system. Figure 4a describes the schematic

DOI: 10.1021/acsnano.5b05286
ACS Nano XXXX, XXX, XXX−XXX

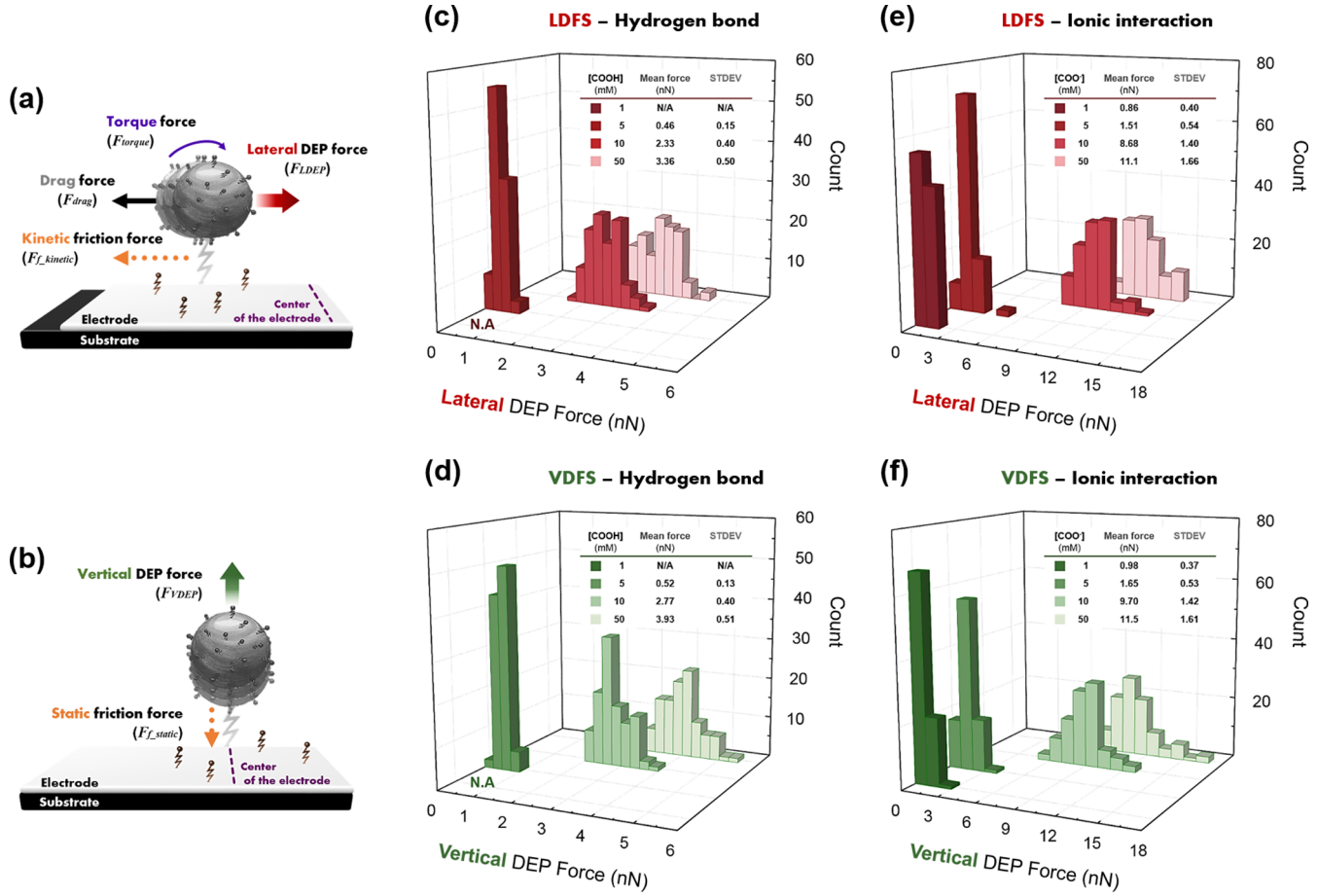

Figure 4. (a,b) Schematic illustration of the BDFS system model: (a) LDFS system when the functionalized bead is moved along the functionalized surface on the electrode; (b) schematic illustration of the VDFS system model when the functionalized bead is levitated on the electrode. (c-f) Histogram and Gaussian fitting graphs as a function of rupture force, rupturing the weak binding interactions as the concentration is varied, and the mean rupture force and standard deviation (insets): (c) hydrogen interaction in the LDFS system; (d) hydrogen interaction in the VDFS system; (e) ionic interaction in the LDFS system; (f) ionic interaction in the VDFS system. The measurement consistency of the BDFS system was also validated by applying the different magnitude of the applied AC signal (see Supporting Figure S7).

diagram during lateral movement of the beads for the developed method. During the lateral movement, the following relationship exists, $F_{LDEP} > F_{drag} + F_{f\_kinetic} + F_{torque}$, where F_{LDEP} is the lateral DEP force, F_{drag} is Stokes' drag force as a function of bead velocity, $F_{f\_kinetic}$ is the kinetic friction force that consists of weak binding interaction forces between the functionalized beads and functionalized surfaces, and F_{torque} is torque force that can be generated by shear force and surface adhesion related to the wall effect as the beads move on the surface. As shown in Figure 2a, as the beads approached the center of the electrode, the lateral DEP force was also reduced, resulting in a velocity decrease for the bead (*e.g.*, Figure 2b). This lead to a reduced Stokes' velocity for the bead. Hence, when the bead stopped at a certain position, the Stokes' drag force and torque were zero (see Supporting Note N4 for detailed description), and $F_{f\_kinetic}$ became the static friction force (F_{f_static}). Hence the lateral DEP force exerted on the bead was equivalent to the weak binding interactions present at the stop position. Using these experimental results, and by calculating the DEP force *via* FEA based simulations, we can extract the weak binding interaction forces under investigation. Figure 4c,e shows the extracted force graphs which depend on the concentration of functional groups on the substrate surface using the LDFS method. In the VDFS system presented in Figure 4b, the following relationship exists as the functionalized beads are separated from the functionalized surface, $F_{VDEP} = F_{f\_static} + F_{gravity}$, where F_{VDEP} is the vertical DEP force and $F_{gravity}$ is the gravitational force on the bead. Since the effect of gravity ($\sim 10^{-13}$ N) is negligible compared to the weak binding forces,[24] the rupture forces of both interactions using measured data from the VDFS method is represented in Figure 4d,f.[25] Interestingly, we found that the mean forces required to rupture the bonds in VDFS are always slightly higher than those in LDFS even though the experimental conditions of both systems were identical.

To further explore this phenomenon, we investigated the relationship between the force-pulling directions and weak binding interactions by using Poisson statistical analysis method with the experimental data in Figure 4. Using the Poisson statistical analysis method (a detailed description of the analytical method can be found in Materials and Methods), the specific number of bonds within the contact area can be extracted from the mean forces and standard deviations in the experimental results (Figure 4 inset tables). The difference between the calculated specific number of bonds in the LDFS and VDFS systems may have originated from differences in

DOI: 10.1021/acsnano.5b05286
ACS Nano XXXX, XXX, XXX−XXX

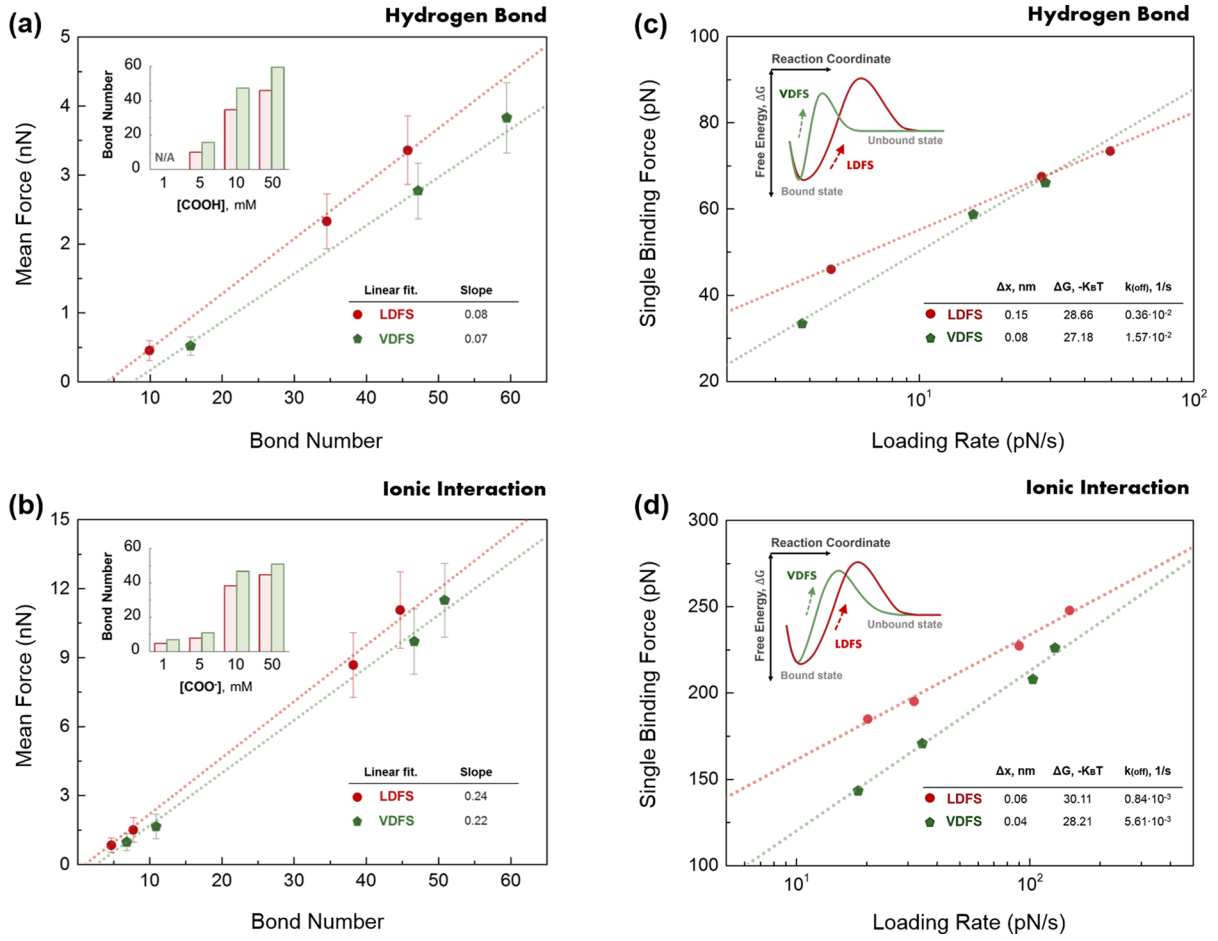

Figure 5. Mean force *vs* number of bonds and the free energy reaction coordinate. (a,b) Result of the mean force *vs* the number of bonds for the LDFS and VDFS. Inset graph: surface-functionalized group concentration *vs* number of bonds. Inset table: value of the linear slope. (a) Hydrogen interactions between carboxyl-terminated beads and the carboxyl-functionalized oxide surface at pH 4 with 5, 10, and 50 mM concentrations. (b) Electrostatic attraction (ionic) bonds between amino-terminated beads and the carboxyl-functionalized oxide surface at pH 7 with 1, 5, 10, and 50 mM concentrations. (c,d) Result of the free energy reaction coordinate with each state. Inset tables: energy barrier width (Δx), energy barrier height (ΔG), natural frequency (k_{off}). Inset graphs: schematic illustration of the energy pathway dependent on the direction of force. (c) Hydrogen bond. (d) Ionic interaction. All adjusted R^2 values in the linear fit are up to 0.98.

movement directions. When the bead moved upward from the surface in the VDFS system, whole numbers of functionalized molecules in the contact area of the bead take part in the rupture event. On the other hand, with lateral movement of the beads, a certain portion of functionalized molecules in the contact region might not have participated in rupture or binding interactions due to rotation of the beads. According to Figure 5a,b, the participating ratio of bonds during hydrogen and ionic rupture events in the LDFS system is always smaller than that of bonds in the VDFS system (~80% in the LDFS system *versus* that in the VDFS system). Another interesting point in Figure 5a,b is the linear relationship between the number of bonds and the mean force value of the weak binding interaction. The linear slopes of the weak binding interaction *via* LDFS and VDFS were 0.08, 0.07 (hydrogen bonds) and 0.24, 0.22 (ionic interactions), respectively. The larger linear slope denoted a slightly higher bond affinity,[26,27] and these results show that the bond affinity of the weak binding interactions relied on the direction of the pulling force.[17,28,29]

In order to verify the potential to examine the participating ratio of bonds and the dependency of the bond affinity to the direction of the pulling force in the BDFS system, we extracted the energy landscape diagrams of hydrogen bonds and ionic interactions along the force direction, utilizing the same measured data presented in Figure 4. Associating single binding forces as a function of the load rate *via* the Bell model (detailed analytical methods can be found in Materials and Methods),[30] the energy landscape diagram of the hydrogen bonds and ionic interactions along the force direction were calculated in Figure 5c,d, resulting in an ascending slope of linear regimes for a single binding force *versus* $\log_e$ (loading rate). The linear regime of each weak binding interaction was different along the force-pulling direction, which is expected given that the energy landscape pathways of the weak binding interactions depend strongly on the direction of the pulling force. The insets in Figure 5c,d show that the energy barrier heights (ΔG) and energy barrier widths (Δx) of the weak binding interactions, even though in the same range as in the prior report,[17] were significantly affected by the force direction. This implies that the BDFS system has the capability to examine the number of bonds and the binding affinity of intermolecular interactions when different force-pulling directions are applied. From Figure 5a,b, the values of the *y*-intercepts of the linear slope are near zero, indicating that the nonspecific interaction between beads and the substrate surface are minimal. Therefore, the natural frequency (k_{off}) can be described *via* the bond affinity, which is

DOI: 10.1021/acsnano.5b05286
ACS Nano XXXX, XXX, XXX−XXX

related to the dissociation rate during a bond rupture event. The natural frequencies of hydrogen and ionic interactions in LDFS are 0.36×10^{-2} and 0.84×10^{-3} (1/s), which are in contrast with the values of 1.57×10^{-2} and 5.61×10^{-3} (1/s) for VDFS, as shown in the insets of Figure 5c,d. This shows that small dissociation rates in bond rupture events correspond with large bond affinities. Moreover, the energy landscapes are tilted to lower energy barriers *via* the force-pulling direction (in VDFS), indicating that the probability of bond survival is lowered while bond dissociation is accelerated.[26,27] This trend is similar to the previous description that bond affinity corresponded with the number of bonds (Figure 5a,b).

CONCLUSION

In conclusion, we reported the application of a biaxial dielectrophoretic force spectroscopy method, which combined lateral dielectrophoretic force spectroscopy with vertical dielectrophoretic spectroscopy within a microfluidic device. In the LDFS system, the lateral movements of functionalized beads across a substrate surface due to rotation was used to investigate weak binding interactions, whereas the VDFS system used vertical movements to examine the particular interactions. Using this system, we measured hydrogen and ionic interactions as a model system, with various pulling directions and loading rates, to rupture the binding interactions between carboxyl- or amino-functionalized beads and carboxyl-functionalized silicon dioxide surfaces under the same environment. From the measured data, it was observed that the difference of bond numbers participating in the rupture events is about 20% lower in the lateral direction *versus* that in the vertical pulling directions. Moreover, the slope in the LDFS system, which was extracted from the linear relationship between the number of bonds and the mean rupture force of the weak binding interaction, was greater than what was measured for the VDFS system, denoting a higher bond affinity in the lateral pulling direction. Lastly, energy barrier widths and heights were calculated from the measured data in the BDFS system in conjunction with the Bell model, resulting in a verification of the existence of different energy pathways denoted by the pulling direction. The dissociation rates of the weak binding interactions extracted from the Bell model and measured data also confirmed the existence of 4−6 times higher bond affinities in the lateral pulling direction. Using the methods in this study provided deeper insight and a better understanding of characteristics such as the number of bonds participating in an interaction, bond affinities, free energy landscapes, and association/dissociation rates as well as providing a demonstration of the simplicity and power of this tool for use in the investigation of weak binding interactions.

MATERIALS AND METHODS

Microchip Fabrication. An interdigitated electrode array pattern was prepared on an oxidized silicon wafer through the lift-off process, where each electrode line was 80 μm wide with a 40 μm gap. A 0.1 μm thick chromium layer was deposited *via* thermal evaporation and subsequently patterned using a lift-off process. The metal electrodes were shielded with a 0.8 μm thick plasma-enhanced chemical vapor deposited silicon dioxide. The electrode contact pads were subsequently prepared *via* wet etching processes to apply voltage to the IDT array (Supporting Note N5).

Preparation of the Carboxyl-Terminated Oxide Surface Layers. The IDT electrode shielded by an oxide layer was immersed into a solution consisting of H_2SO_4/H_2O_2 (3:7), resulting in the formation of a hydroxyl-functionalized substrate (SiO_2−OH). The hydroxyl-functionalized substrate was discretely placed into a 1, 5, 10, and 50 mM solution of 3-aminopropyltriethoxysilane (A3648, Sigma-Aldrich, St. Louis, MO, USA) solution in ethanol for 80 min, resulting in an amino-functionalized substrate (SiO_2−NH_2). This amino-functionalized substrate was immersed in 0.1 M succinic anhydride (239690, Sigma-Aldrich) in DMF (*N*,*N*-dimethylformamide, D158550, Sigma-Aldrich) for 24 h. The chip with carboxyl-functional groups on its surface (SiO_2−COOH) was washed with DMF and DI water and dehydrated with nitrogen gas[31] (see Supporting Note N6 for detailed density quantification of the surface functional group).

Functionalization of Microbeads. Functionalized polystyrene microbeads (carboxyl-terminated beads and amino-terminated microbeads) used in the experiments were purchased from Spherotech Inc. (Libertyville, IL, USA), and the original stock solution containing the microbeads contained PBS buffer (pH 7.4) stabilized with 0.02% sodium azide. For the experiments, the stock solutions were diluted with DI water as follows: 1.8 mL of DI water + 15 μL of the 10 μm bead stock solution. After dilution, the concentration of beads in the diluted solution was $\sim 5 \times 10^5$ particles/mL.

Experimental Setup. The silicon dioxide surface inside the chip was functionalized using each molecule. A PDMS (polydimethylsiloxane) layer was used to form an open reservoir above the chip. Commercially available functionalized polystyrene beads suspended in DI water were poured into the reservoir. Next, a cover glass slide was used to cover the top of PDMS reservoir. For high-voltage applications, a sinusoidal signal at 1 kHz to 1 MHz with 0−300 V peak-to-peak voltages was applied to the chip using an amplifier (WMA-300, Falco Systems, Amsterdam, The Netherlands) that was already interconnected to the function generator. The amplitude and frequency of the signal generated by the function generator or the amplifier was rechecked with an oscilloscope (WaveRunner 6050, LeCroy, New York, NY, USA) for the confirmation. By applying the sinusoidal signal at various voltage levels and loads, movement of the beads was observed and recorded with top-view microscopes, which were connected to high-speed CCD cameras (Motion Scope M3, Redlake, San Diego, CA, USA) with Frame-Grabber (Xcelera-CL PX4 Dual, Teledyne DALSA, Co., Waterloo, ON, Canada), simultaneously. Images were acquired at 1−100 frame/s for each experimental condition, and bead movement was tracked *via* ImageJ software (NIH, USA) with a particle tracker and detector plug-in.[32]

Method for Converting Applied Voltage to DEP Force in Earlier Papers. The total DEP force is given by

$$\vec{F}_{\text{total}} = \sum_{0}^{\infty} -\nabla U_n,$$
$$U_n = -\frac{2\pi\varepsilon_m K_n r^{(2n+1)}}{(2n+1)!!} \sum_{i+j+k=n} \frac{1}{i!j!k!}\left[\frac{\partial^n \Phi}{\partial x^i \partial y^j \partial z^k}\right]^2,$$
$$K_n = \frac{n(2n+1)(\tilde{\varepsilon}_p - \tilde{\varepsilon}_m)}{n\tilde{\varepsilon}_p + (n+1)\tilde{\varepsilon}_m} \quad (1)$$

where n is the force order, Φ refers to the electrostatic potential of the external electric field, and K_n is the nth-order Clausius−Mossotti factor.[23−25,33] Based on this equation, the total DEP force was calculated from a custom-built code run on MATLAB (2010a, Mathworks, USA). The electrical field profiles for the IDT electrodes used in the experiment, when the AC signal with 1 V to 300 $V_{p\text{-}p}$ and 1 kHz to 1 MHz was applied to the electrodes, were generated from a finite element program (v3.5a, COMSOL Multiphysics) with a grid spacing of 0.2 μm. The experimental parameters and the generated electric field data were used as inputs for the MATLAB code. Consequently, the DEP force could be calculated depending on the applied voltage. It should be noted that the effect of electrothermal forces generated by the applied voltage can be neglected in the system (see Supporting Note N7). Hence, we only consider the DEP force acting on the functionalized beads when the voltage is applied into the system.

Calculation of the Gravitational Force on the Beads in the System. The formula for calculating the force of gravity may be

DOI: 10.1021/acsnano.5b05286
ACS Nano XXXX, XXX, XXX−XXX

written as $\frac{4}{3}\pi r^3(\rho_p - \rho_m)g)$, where r (5 μm) is the radius of the bead, ρ_p (1.03×10^3 kg/m^3) and ρ_m (1×10^3 kg/m^3) are the densities of the bead and media, and g (9.8 m/s^2) is the gravitational acceleration constant. As a result, the gravitational force on the microbeads is about ~0.1 pN.

Method for Calculating an Individual Bond Using Poisson Statistics. Bond formation between a microbead and the substrate surface should vary with measurement conditions such as molecular density, contact area, and so on. The Poisson statistical method is able to minimize the difference between the measured conditions and extracts the binding strength of the individual. For Poisson statistical analysis, it is assumed that the individual bond is discrete random variables and the rupture force between the surface and the probe is the sum of the binding of the individual. According to previous reports, these assumptions are considered to be reasonable.[34,35] Poisson distribution is the probability of observing a random sample of n discrete events (*i.e.*, n events to cause the rupture of an individual bond), and the rupture force should vary as a Poisson distribution with the following mean (m) and variance (σ^2):

$$m = nF \text{ and } \sigma^2 = nF \tag{2}$$

where F and n are the binding force of each of the stationary contact areas and the number of individual bonds, respectively. Then, the individual binding force can be described as

$$F = \frac{\sigma^2}{m} \tag{3}$$

Estimating Energy Barrier Height and Width Based on Kinetic theory. The Arrhenius equation $\Delta G = -k_B T \cdot \ln(k_{off}/k_A)$ was used to analyze the energy barrier height, ΔG, where k_{off} denotes the natural frequency, k_B is the Boltzmann constant, T is the absolute temperature, and k_A is the Arrhenius frequency factor (in noncovalent interactions, $k_A = \sim 10^9$ s^{-1}).[17] Slopes of linear regimes for single binding forces *versus* logarithmic loading rates reflect the energy barrier. Based on Bell theory, $F_s = (k_B T/\Delta x) \cdot \ln((\Delta x/r_f)/(k_{off} k_B T))$, the logarithmic x-intercept denotes the natural frequency, k_{off}, and each slope represents the force scale $f = k_B T/\Delta x$, where F_s, Δx, and r_f are the single binding force, energy barrier width, and loading rate, respectively.[17,30]

ASSOCIATED CONTENT

Supporting Information

The Supporting Information is available free of charge on the ACS Publications website at DOI: 10.1021/acsnano.5b05286.

Additional figures, experimental details, and movie descriptions (PDF)
Movie M1 (AVI)
Movie M2 (AVI)
Movie M3 (AVI)

AUTHOR INFORMATION

Corresponding Author

*E-mail: yusuklee@yonsei.ac.kr.

Author Contributions

▼I.S.P. and T.J.K. contributed equally to this work.

Notes

The authors declare no competing financial interest.

ACKNOWLEDGMENTS

This research was supported by Basic Science Research Program through the National Research Foundation of Korea (NRF) funded by the Ministry of Science, ICT & Future Planning (NRF-2013R1A2A2A03005767, NRF-2013R1A1A2053613), Republic of Korea, and by the Yonsei University Future-leading Research Initiative of 2015 (2015-22-0059).

REFERENCES

(1) Bustamante, C.; Chemla, Y. R.; Forde, N. R.; Izhaky, D. Mechanical Processes in Biochemistry. *Annu. Rev. Biochem.* **2004**, *73*, 705−748.
(2) Wang, X.; Ha, T. Defining Single Molecular Forces Required to Activate Integrin and Notch Signaling. *Science* **2013**, *340*, 991−994.
(3) Bustamante, C.; Rivetti, C.; Keller, D. J. Scanning Force Microscopy under Aqueous Solutions. *Curr. Opin. Struct. Biol.* **1997**, *7*, 709−716.
(4) Ros, R.; Schwesinger, F.; Anselmetti, D.; Kubon, M.; Schäfer, R.; Plückthun, A.; Tiefenauer, L. Antigen Binding Forces of Individually Addressed Single-Chain Fv Antibody Molecules. *Proc. Natl. Acad. Sci. U. S. A.* **1998**, *95*, 7402−7405.
(5) Liang, M. N.; Smith, S. P.; Metallo, S. J.; Choi, I. S.; Prentiss, M.; Whitesides, G. M. Measuring the Forces Involved in Polyvalent Adhesion of Uropathogenic Escherichia Coli to Mannose-Presenting Surfaces. *Proc. Natl. Acad. Sci. U. S. A.* **2000**, *97*, 13092−13096.
(6) Moffitt, J. R.; Chemla, Y. R.; Izhaky, D.; Bustamante, C. Differential Detection of Dual Traps Improves the Spatial Resolution of Optical Tweezers. *Proc. Natl. Acad. Sci. U. S. A.* **2006**, *103*, 9006−9011.
(7) Gosse, C.; Croquette, V. Magnetic tweezers: Micromanipulation and Force Measurement at the Molecular Level. *Biophys. J.* **2002**, *82*, 3314−3329.
(8) Zhu, R.; Howorka, S.; Pröll, J.; Kienberger, F.; Preiner, J.; Hesse, J.; Ebner, A.; Pastushenko, V. P.; Gruber, H. J.; Hinterdorfer, P. Nanomechanical Recognition Measurements of Individual DNA Molecules Reveal Epigenetic Methylation Patterns. *Nat. Nanotechnol.* **2010**, *5*, 788−791.
(9) Bell, G. Models for the Specific Adhesion of Cells to Cells. *Science* **1978**, *200*, 618−627.
(10) McEver, R. P.; Zhu, C. Rolling Cell Adhesion. *Annu. Rev. Cell Dev. Biol.* **2010**, *26*, 363−396.
(11) Rief, M.; Gautel, M.; Oesterhelt, F.; Fernandez, J. M.; Gaub, H. E. Reversible Unfolding of Individual Titin Immunoglobulin Domains by AFM. *Science* **1997**, *276*, 1109−1112.
(12) Eom, K.; Makarov, D. E.; Rodin, G. J. Theoretical Studies of the Kinetics of Mechanical Unfolding of Cross-Linked Polymer Chains and Their Implications for Single-Molecule Pulling Experiments. *Phys. Rev. E* **2005**, *71*, 021904.
(13) Borgia, A.; Williams, P. M.; Clarke, J. Single-Molecule Studies of Protein Folding. *Annu. Rev. Biochem.* **2008**, *77*, 101−125.
(14) Zlatanova, J.; Lindsay, S. M.; Leuba, S. H. Single Molecule Force Spectroscopy in Biology using the Atomic Force Microscope. *Prog. Biophys. Mol. Biol.* **2000**, *74*, 37−61.
(15) Greenleaf, W. J.; Woodside, M. T.; Block, S. M. High-Resolution, Single-Molecule Measurements of Biomolecular Motion. *Annu. Rev. Biophys. Biomol. Struct.* **2007**, *36*, 171−190.
(16) Williams, P. M. Analytical Descriptions of Dynamic Force Spectroscopy: Behavior of Multiple Connections. *Anal. Chim. Acta* **2003**, *479*, 107−115.
(17) Dietz, H.; Berkemeier, F.; Bertz, M.; Rief, M. Anisotropic Deformation Response of Single Protein Molecules. *Proc. Natl. Acad. Sci. U. S. A.* **2006**, *103*, 12724−12728.
(18) Carrion-Vazquez, M.; Li, H.; Lu, H.; Marszalek, P. E.; Oberhauser, A. F.; Fernandez, J. M. The Mechanical Stability of Ubiquitin is Linkage Dependent. *Nat. Struct. Biol.* **2003**, *10*, 738−743.
(19) Best, R. B.; Paci, E.; Hummer, G.; Dudko, O. K. Pulling Direction as a Reaction Coordinate for the Mechanical Unfolding of Single Molecules. *J. Phys. Chem. B* **2008**, *112*, 5968−5976.
(20) Mickler, M.; Dima, R. I.; Dietz, H.; Hyeon, C.; Thirumalai, D.; Rief, M. Revealing the Bifurcation in the Unfolding Pathways of GFP by Using Single-Molecule Experiments and Simulations. *Proc. Natl. Acad. Sci. U. S. A.* **2007**, *104*, 20268−20273.
(21) Rico, F.; Moy, V. T. Energy Landscape Roughness of the Streptavidin-Biotin Interaction. *J. Mol. Recognit.* **2007**, *20*, 495−501.

DOI: 10.1021/acsnano.5b05286
ACS Nano XXXX, XXX, XXX−XXX

(22) Maitra, A.; Arya, G. Model Accounting for the Effects of Pulling-Device Stiffness in the Analyses of Single-Molecule Force Measurements. *Phys. Rev. Lett.* **2010**, *104*, 108301.
(23) Lee, S. W.; Li, H.; Bashir, R. Dielectrophoretic Tweezers for Examining Particle-Surface Interactions within Microfluidic Devices. *Appl. Phys. Lett.* **2007**, *90*, 223902.
(24) Baek, S. H.; Chang, W. J.; Baek, J. Y.; Yoon, D. S.; Bashir, R.; Lee, S. W. Dielectrophoretic Technique for Measurement of Chemical and Biological Interactions. *Anal. Chem.* **2009**, *81*, 7737−7742.
(25) Park, I. S.; Eom, K.; Son, J.; Chang, W. J.; Park, K.; Kwon, T.; Yoon, D. S.; Bashir, R.; Lee, S. W. Microfluidic Multifunctional Probe Array Dielectrophoretic Force Spectroscopy with Wide Loading Rates. *ACS Nano* **2012**, *6*, 8665−8673.
(26) Kuo, S. C.; Lauffenburger, D. A. Relationship between Receptor/Ligand Binding Affinity and Adhesion Strength. *Biophys. J.* **1993**, *65*, 2191−2200.
(27) Cozens-Roberts, C.; Quinn, J. A.; Lauffenberger, D. A. Receptor-Mediated Adhesion Phenomena. Model Studies with the Radical-Flow Detachment Assay. *Biophys. J.* **1990**, *58*, 107−125.
(28) Rajesh, R.; Giri, D.; Jensen, I.; Kumar, S. Role of Pulling Direction in Understanding the Energy Landscape of Proteins. *Phys. Rev. E* **2008**, *78*, 021905.
(29) Guinn, E. J.; Jagannathan, B.; Marqusee, S. Single-Molecule Chemo-Mechanical Unfolding Reveals Multiple Transition State Barriers in a Small Single-Domain Protein. *Nat. Commun.* **2015**, *6*, 6861.
(30) Merkel, R.; Nassoy, P.; Leung, A.; Ritchie, K.; Evans, E. Energy Landscapes of Receptor−Ligand Bonds Explored with Dynamic Force Spectroscopy. *Nature* **1999**, *397*, 50−53.
(31) An, Y.; Chen, M.; Xue, Q.; Liu, W. Preparation and Self-Assembly of Carboxylic Acid-Functionalized silica. *J. Colloid Interface Sci.* **2007**, *311*, 507−513.
(32) Feng, Y.; Goree, J.; Liu, B. Accurate Particle Position Measurement from Images. *Rev. Sci. Instrum.* **2007**, *78*, 053704.
(33) Jones, T. B. Basic Theory of Dielectrophoresis and Electrorotation. *Engin. in Med. Bio. Mag.* **2003**, *22*, 33−42.
(34) Williams, J. M.; Han, T.; Beebe, T. P., Jr. Determination of Single-Bond Forces from Contact Force Variances in Atomic Force Microscopy. *Langmuir* **1996**, *12*, 1291−1295.
(35) Wenzler, L. A.; Moyes, G. L.; Olson, L. G.; Harris, J. M.; Beebe, T. P., Jr. Single-Molecule Bond-Rupture Force Analysis of Interactions between AFM Tips and Substrates Modified with Organosilanes. *Anal. Chem.* **1997**, *69*, 2855−2861.

DOI: 10.1021/acsnano.5b05286
ACS Nano XXXX, XXX, XXX−XXX